

## ARTICLE OPEN



# PRAS40 promotes colorectal cancer stemness by enhancing glycolysis through triggering PGK1 acetylation

Chengfei Zhang<sup>1,6</sup>, Yufei Bo<sup>1,6</sup>, Ting Zhang<sup>1,2</sup>, Xinran Chen<sup>1</sup>, Tianhua Zhang<sup>1,2</sup>, Hongming Teng<sup>1,2</sup>, Yue Wang<sup>1,2</sup>, Yuanyuan Luo<sup>1,2</sup>, Jinghua Sun<sup>3</sup>, Lihui Wang<sup>4</sup>, Xiuli Wang<sup>5</sup> and Lin Huang<sup>1,2</sup>

© The Author(s) 2025

Cancer stem cells (CSCs) play a pivotal role in driving colorectal cancer (CRC) progression and therapeutic resistance. However, the molecular mechanisms regulating CRC-CSC properties are not fully understood. Proline-rich Akt substrate 40 (PRAS40) is involved in various tumorigenic processes, yet little is known about its contribution to cancer stemness. In this study, we demonstrated that PRAS40 was overexpressed in CRC tissues and its elevated expression positively correlated with poor patient survival. Genetic ablation of PRAS40 suppressed tumorigenesis in CRC mouse models. Notably, PRAS40 enhanced the stemness of CRC cells, as evidenced by increased sphere formation, upregulation of stem cell markers, enrichment of the CD133<sup>+</sup>CD44<sup>+</sup> cell population, and enhanced tumor initiation capacity in vivo. Mechanistically, PRAS40 induced a glycolytic phenotype by interacting with and activating the glycolytic enzyme phosphoglycerate kinase 1 (PGK1). Furthermore, PRAS40 enhanced the interaction between PGK1 and the acetyltransferase p300/CBP-associated factor (PCAF), thereby promoting PGK1 acetylation, which contributes to glycolysis activation and the maintenance of CRC stemness. Pharmacological inhibition of acetylation attenuated PRAS40-mediated CRC stemness and colorectal carcinogenesis. Collectively, our findings uncover a novel PRAS40/PGK1 regulatory axis that promotes CRC stemness and tumorigenesis through enhanced glycolysis, suggesting potential therapeutic strategies targeting this axis for CRC treatment.

*Oncogenesis* (2026)15:2; <https://doi.org/10.1038/s41389-025-00594-x>

## INTRODUCTION

Colorectal cancer (CRC) has become the first-leading cause of cancer death in men and the second-leading cause in women younger than 50 years old in the USA, while its incidence and mortality rates have significantly increased recently in China [1, 2]. Although advances in treatment have improved overall survival in CRC, outcomes remain poor for many patients, particularly those with advanced or metastatic disease [3, 4]. Cancer stem cells (CSCs), a subpopulation of cancer cells with high proliferative and tumorigenic potential, are widely considered responsible for tumor persistence and therapeutic resistance [5]. In CRC, the existence of CSCs has been firmly established, with several surface markers such as CD44, CD133/PROM1, LGR5, etc used for their identification. CSCs are now recognized as a major source of CRC heterogeneity, cancer progression, chemoresistance, and therapeutic failure [6–8]. Therefore, targeting CSCs represents a promising strategic direction for therapy. Several agents directed against CSCs have already entered clinical trials for various cancer types [9].

CSCs exhibit unique metabolic flexibility, contributing to the maintenance of their characteristics [10]. A key feature is their preferential reliance on glycolysis, characterized by increased glucose uptake, upregulated and activated glycolytic enzymes,

and elevated lactate production [11–16]. Consequently, inhibiting glycolysis suppresses the maintenance of CSC population. For instance, the glucose-analog 2-deoxy-D-glucose (2-DG) remarkably suppresses sphere formation and tumor xenograft growth in breast and liver cancers [12, 16, 17]. Targeting peroxisome-proliferator-activated receptor  $\alpha$  (PPAR $\alpha$ ) inhibited glycolysis, resulting in significant toxicity to leukemia stem-like cells [18]. Upregulation of glycolytic factors such as GLUT1, HK2, PKM2, and LDHA is observed in colorectal cancer, and contributes to CSC maintenance [17, 19]. However, the precise underlying mechanisms warrants further elucidation. Proline rich Akt substrate 40 (PRAS40), encoded by *AKT1S1*, is a substrate of Akt1 and a constituent of mTOR complex 1 (mTORC1) [20–23]. Accumulating evidence from our group and others demonstrate that PRAS40 promotes cell survival, proliferation, and metastasis, while suppressing cell death and autophagy in various cancers [24–26]. However, its role in colorectal carcinogenesis remains elusive, and whether PRAS40 affects cancer stemness warrants further investigation. PRAS40 mRNA expression has been reported to positively correlate with the expression of glycolytic hallmarks in clear cell renal cell carcinoma (ccRCC), though the influence of PRAS40 on glycolysis remains undetermined [27].

<sup>1</sup>Department of Pathophysiology, College of Basic Medical Sciences, Dalian Medical University, 9 South Lvshun Road, Dalian, Liaoning 116044, China. <sup>2</sup>Liaoning Provincial Key Laboratory of Medical Cellular and Molecular Biology, 9 South Lvshun Road, Dalian, Liaoning 116044, China. <sup>3</sup>Department of Medical Oncology, The Second Hospital of Dalian Medical University, Dalian, Liaoning 116023, China. <sup>4</sup>Department of Pathology, School of Medicine, Jinan University, Guangzhou 510632, China. <sup>5</sup>Histology & Embryology Department, Dalian Medical University, 9 South Lvshun Road, Dalian, Liaoning 116044, China. <sup>6</sup>These authors contributed equally: Chengfei Zhang, Yufei Bo. ✉email: wanglh@jnu.edu.cn; Panpan1210\_dmu@163.com; lhuang@dmu.edu.cn

Received: 15 September 2025 Revised: 21 November 2025 Accepted: 3 December 2025

Published online: 27 December 2025

**Table 1.** Correlation of PRAS40 expression to clinicopathological variables in CRC patients of Cohort 1.

Variables	PRAS40 expression		P value*
	Low level (%)	High level (%)	
Total (n = 75)	18 (24.0)	57 (76.0)	
Sex			
Male (n = 42)	8 (19.0)	34 (81.0)	0.287
Female (n = 33)	10 (30.3)	23 (69.7)	
Tumor size (cm)			
>5 (n = 41)	11 (26.8)	30 (73.2)	0.595
>5 (n = 34)	7 (20.6)	27 (79.4)	
Grade			
I-II (n = 58)	14 (24.1)	44 (75.9)	1.000
III-IV (n = 17)	4 (23.5)	13 (76.5)	
Age (years)			
≤66 <sup>△</sup> (n = 34)	11 (32.4)	23 (67.6)	0.175
>66 (n = 41)	7 (17.1)	34 (82.9)	
PDL1 (H-score)			
>120 <sup>▽</sup> (n = 64)	16 (25.0)	48 (75.0)	1.000
>120 (n = 11)	2 (18.2)	9 (81.8)	
TNM stage			
I (n = 8)	5 (62.5)	3 (37.5)	
II (n = 17)	2 (11.8)	15 (88.2)	<b>0.017</b>
III (n = 26)	4 (15.4)	22 (84.6)	<b>0.017</b>
IV (n = 20)	3 (15.0)	17 (85.0)	<b>0.022</b>
V (n = 4)	4 (100.0)	0 (0.0)	0.49

Stage I, T1-T2N0M0; stage II, T3N0M0; stage III, T4N0M0; stage IV, any T any NM0; stage V, any T any NM1. \*Fisher's exact test. <sup>△</sup>Mean age. <sup>▽</sup>Median H-score. Significant P-values are shown in bold.

Previously, we reported that the glycolytic enzyme phosphoglycerate kinase 1 (PGK1) phosphorylates PRAS40 to inhibit autophagy-mediated cell death. However, whether PRAS40 reciprocally modulates PGK1's function remained uncharacterized [25]. PGK1 catalyzes the conversion between 1, 3-bisphosphoglycerate and 3-phosphoglycerate, and is overexpressed in various cancers, including CRC, pancreatic cancer, and hepatocellular carcinoma (HCC) [28–30]. Beyond its metabolic role, PGK1 promotes tumorigenesis as a protein kinase. Its oncogenic capacity is further regulated by diverse posttranslational modifications that fine-tune glycolytic flux and support malignant progression. For example, K323 acetylation and Y324 phosphorylation of PGK1 enhance its enzymatic activity, promoting glycolysis in cancer cells [29, 31, 32]. Similarly, R206 methylation increases its S203 phosphorylation, while S203 phosphorylation and T255 O-GlcNAcylation of PGK1 suppress oxidative phosphorylation and favor glycolysis in cancer cells [28, 33, 34]. Moreover, PGK1 has been implicated in triggering cancer stemness. In liver cancer stem cells, its mitochondrial import reprograms the metabolism from oxidative phosphorylation to glycolysis, improving self-renewal capacity [15]. In breast cancer cells, PGK1 contributes to cancer stemness by increasing serine synthesis or interacting with HSP90 to stabilize GSK3 $\beta$  expression [35, 36]. Despite these advances, the role of PGK1 in regulating CRC stemness and whether this is mediated by its glycolytic function remain elusive.

In this study, our data suggest that PRAS40 promotes colorectal carcinogenesis by enhancing the stemness of colon cancer cells. As a mechanism, PRAS40 facilitates PGK1's activity via increasing

PGK1 acetylation, consequently facilitating glycolysis. Our results provide a potential therapeutic strategy for CRC via targeting the PRAS40/PGK1 axis.

## MATERIALS AND METHODS

### Patient samples

Tissue arrays HCoIA160CS01 (n = 75, Cohort 1) and HCoIA180Su18 (n = 91, Cohort 2) containing primary cancer tissue and the corresponding adjacent peri-cancer tissue were purchased from Shanghai Outdo Biotech Co., Ltd. No preoperative anticancer treatments were received (Table 1, Supplementary Tables 1, 2). The experimental protocols were approved by the ethics committee of the company (SHYJS-CP-1701008), and all the materials were sufficiently anonymised.

### Mice

The protocol of animal experiments was approved by the Animal Care and Ethics Committee of Dalian Medical University (AEE22084). All animal maintenance and procedures were carried out following the recommendations by the Animal Care and Ethics Committee of Dalian Medical University. Mice were maintained in a temperature- and humidity-controlled room on a 12-h light/dark cycle at Specific Pathogen Free Experimental Animal Center of Dalian Medical University.

The *Akt1s1* knockout mice were created using CRISPR/Cas9 system by Beijing Biocytogen (Beijing, China). The exons 2–5 at the *Akt1s1* locus in the mouse genome encompassing the entire coding sequence were deleted, which was positively confirmed by sequencing of PCR products. The genotypes of *Akt1s1* knockout mice were confirmed by PCR using primers MSD-F and MSD-R for wild type alleles and primers MSD-F and MSD-R1 for mutant alleles (Supplementary Table 3).

### Antibodies and reagents

Antibodies were purchased for detection of PRAS40 (26915), PCNA (13110), PCAF (3378 T) (Cell Signaling); PGK1 (17811-1-AP), CD133 (66666-1-Ig),  $\alpha$ -Tubulin (66031-1-Ig),  $\beta$ -Actin (66009-1-Ig), CD44 (15675-1-AP) (Proteintech); SIRT7 (ab259968), anti-phosphotyrosine (ab179530) (Abcam); and pan-Acetyl (sc-8649)(Santa Cruz Biotechnology). Azoxymethane (AOM), Polybrene and 2-DG were from Sigma-Aldrich; dextran sodium sulfate (DSS) was from MP Biomedicals; PU139 and anacardic acid were from TOPSCIENCE.

### CRC mouse models

The 6–8-week-old male mice (13 *Akt1s1*<sup>+/+</sup> mice and 17 *Akt1s1*<sup>-/-</sup> mice) were injected intraperitoneally with azoxymethane (10 mg/kg). One week later, mice were subjected to three cycles of DSS treatment, with each cycle consisting of the administration of 2% DSS for 5 days followed by a 14-day recovery period with regular water. Twenty weeks after the AOM injection, the mice were dissected by technicians blinded to the treatment groups.

### Cell lines and cell culture

Human colon cancer cell lines HT29, HCT116 and SW480, and human embryo kidney cell line 293T were obtained from the Cell Resource Center, Peking Union Medical College, and underwent testing for eight STR loci and the amelogenin gene. All cell lines tested negative for mycoplasma. SW480 and HEK293T were grown in Dulbecco's Modified Eagle's medium, and HCT116 were grown in McCoy's 5A Medium (modified), supplemented with 10% fetal bovine serum (FBS). HT29 were grown in Dulbecco's Modified Eagle's medium: Nutrient Mixture F-12 (1:1) supplemented with 5% FBS. All the cell lines were incubated at 37 °C with 5% CO<sub>2</sub>.

### Lentivirus production and transduction

Virus particles were harvested 48 h after expression vector transfection with packaging plasmid psPAX2 (a gift from Dr. Didier Trono, Addgene plasmid #12260) and envelope plasmid pMD2.G (a gift from Dr. Didier Trono, Addgene plasmid #12259) into HEK293T cells. Cells were infected with lentivirus at the presence of 8  $\mu$ g/mL of Polybrene.

### Sphere formation assays

The spheres of colon cancer cells were cultured in the corresponding media containing 2% B27, 1% N2, 20 ng/mL bFGF, 20 ng/mL EGF, and

plated in 6-well ultra-low attachment plates. The growth factors were replenished every 3 days. 5-day-old spheres as primary spheres were harvested, digested using accutase, and then regrown for another 5 days, which were defined as secondary spheres. The number and the pictures of secondary spheres were obtained.

### In vivo tumorigenicity assays

The cells transfected with the indicated expression vectors (PRAS40 shRNA expression vector or its negative control vector; PRAS40 overexpression vector or the corresponding empty vector control) were injected subcutaneously into the posterior flanks of 4–5 male BALB/c nude mice at the indicated cell number (Vital River, Beijing). We measured the sizes of tumors with a caliper every 2–3 days. For PU139 treatment, mice were randomly divided into different groups when tumor xenografts became palpable (tumor diameter reached ~5 mm), and PU139 (5 or 10 mg/kg) was peritumorally injected once every 2 days from day 8. The tumor volume was calculated by the formula  $V = 1/2 (\text{width}^2 \times \text{length})$ , and the humane endpoint for tumor burden was set at 1500 mm<sup>3</sup>. Mice were sacrificed 26–28 days after tumor implantation. Tumors were subsequently dissected and weighed by technicians blinded to the treatment group assignments.

### Co-IP

Cell extracts were incubated with anti-FLAG M2 Affinity Gel (Sigma), or anti-PGK1 antibody or control IgG together with protein A agarose (GE) at 4°C overnight, and immunoprecipitates were then subjected to Western blotting assay.

### Measurement of PGK1 activity

The measurement of PGK1 activity using 3-PG as a substrate (the reverse reaction) was performed by incubating cell lysate in 100 µL reaction buffer (50 mM Tris at pH 7.5, 5 mM MgCl<sub>2</sub>, 10 mM 3-PG, 0.2 mM NADH, 5 mM ATP and GAPDH) at 37°C for 30 min and the absorbance was read at 340 nm.

### Immunohistochemical staining

Sections were deparaffinized and dehydrated. After being incubated with 3% hydrogen peroxide for 30 min, antigen retrieval was performed in citric acid buffer in a pressure cooker for 5 min. Slides were incubated with primary antibody (PRAS40, 1:400; PCNA, 1:8000; CD44, 1:100; CD133, 1:50) overnight at 4°C followed by incubation with HRP conjugated secondary antibodies for 1 h at room temperature. Signals were detected using a diaminobenzidine substrate kit, and slides were counterstained with hematoxylin.

Stained sections were scored separately by two investigators blinded to the clinical parameters through multiplying the intensity (0–3) and extent (0–100) of staining as previously described by Wu et al. [37], which were recorded as H-scores. PRAS40 high expression, H-score ≥150; PRAS40 low expression, H-score <150.

### Flow cytometry analyses

Cells were incubated with the primary antibodies (CD44 1:200, CD133 1:50) at room temperature for 60 min, followed with the incubation of secondary antibody for another 60 min. After washing, the cells were resuspended in PBS, and applied to BD Accuri C6 Plus flow cytometer according to the manufacturer's instructions. Data acquisition was performed using software FlowJo. Fluorescence minus one (FMO) controls and unstained cells were included in every experiment to define background fluorescence and set appropriate gating thresholds for each fluorochrome. Subsequent data analysis involved gating on the intact cell population based on forward scatter (FSC) and side scatter (SSC) profiles to exclude debris, followed by selection of single cells using FSC-height versus FSC-area to exclude aggregates. CD44<sup>+</sup>CD133<sup>+</sup> cells were identified based on the fluorescence thresholds set by the FMO controls.

### Statistical analyses

Data were presented as mean ± standard deviation (SD). Differences between groups were assessed by two-sided Student's t-test. Survival rates were acquired by Kaplan-Meier analysis, and survival curves were compared with a log-rank test. For in vitro experiments, all experiments were repeated thrice. GraphPad Prism 8 software was used for all statistical analyses, and  $P < 0.05$  was considered statistically significant.

## RESULTS

### PRAS40 accelerates colorectal carcinogenesis

To identify the role of PRAS40 in CRC, we first studied the RNA sequencing data of COAD (Colon Cancer) and READ (Rectal Cancer) from The Cancer Genome Atlas database (TCGA) and microarray analysis data (GSE89076) from The Gene Expression Omnibus database. The mRNA levels of *AKT1S1* which encodes PRAS40, were significantly higher in cancer tissues compared to peri-cancer tissues (Fig. 1A, B). Next, we examined the protein levels of PRAS40 in two independent clinical cohorts (a set of 75 CRC tissues and 67 corresponding peri-cancer tissues for cohort 1, and a set of 91 CRC tissues and 80 corresponding peri-cancer tissues for cohort 2) by immunohistochemical staining (Table 1, Supplementary Tables 1, 2). The H-scores of PRAS40 staining, calculated based on staining intensity and extent, were higher in cancer tissues compared to matched peri-cancer tissues (Fig. 1C–E). Furthermore, high expression of PRAS40 positively correlated to elevated tumor stage and poor overall survival of CRC patients (Table 1 and Fig. 1F).

To further investigate the effects of PRAS40 on colorectal carcinogenesis, we generated PRAS40 global knockout mice (*Akt1s1*<sup>-/-</sup>) (Fig. 1G, H). PRAS40 deletion notably reduced tumor burden in CRC model mice, manifested by decreased tumor number and size (Fig. 1I–K). Smaller histological lesions and lower PCNA staining were also observed in the cancer regions of *Akt1s1*<sup>-/-</sup> mice (Fig. 1L–N). Collectively, these data suggest that PRAS40 promotes colorectal carcinogenesis.

### PRAS40 enhances the stemness of CRC-CSCs

To explore the mechanism by which PRAS40 promotes colorectal carcinogenesis, we investigated angiogenesis by examining CD31 expression and apoptosis with TUNEL assay in mouse CRC tissues. However, neither angiogenesis nor apoptosis was altered in PRAS40 knockout mice (Supplementary Fig. 1). We further studied the influence of PRAS40 on the viability of colon cancer cell lines, and the viability of monolayer cultures only changed slightly in PRAS40-depleted or PRAS40-overexpressing HT29, HCT116, and SW480 cells, which did not correspond to the suppression of colorectal carcinogenesis observed in PRAS40-deleted mice (Supplementary Fig. 2).

We next questioned whether PRAS40 improved colorectal carcinogenesis by enhancing the stemness of CRC-CSCs. We performed sphere culture using colon cancer cell lines, in which the expression of CD44, CD133/PROM1 and LGR5 was upregulated. Simultaneously, PRAS40 expression was significantly increased in these stem-like cells (Fig. 2A, B, Supplementary Fig. 3). Furthermore, PRAS40 depletion downregulated the expression of CD133, CD44, CD166, ALDH2 and DCLK1, decreased the proportion of CD133<sup>+</sup>CD44<sup>+</sup> cells, and inhibited sphere formation (Fig. 2C–E, Supplementary Fig. 4A). Based on these in vitro results, we explored whether PRAS40 depletion suppresses the tumor-initiating frequency in mice. The growth and weight of CRC xenografts formed by different number of HCT116 cells were substantially inhibited by PRAS40 depletion. Notably, all mice injected with 6 × 10<sup>5</sup> control cells formed tumors (4/4), whereas no tumors formed in the mice injected with PRAS40-depleted cells (0/4) (Fig. 2F–H). The expression of CD133 and CD44 was significantly reduced in the tumors formed by PRAS40-depleted cells (Fig. 2I). In contrast, PRAS40 overexpression upregulated the expression of CD133, CD44, CD166, ALDH2 and DCLK1, increased the proportion of CD133<sup>+</sup>CD44<sup>+</sup> cells, enhanced sphere formation, increased CD44 and CD133 expression in sphere-cultured cells, facilitated tumor-initiating frequency in mice, and upregulated CD44 and CD133 expression in these xenograft tumors (Fig. 2J–Q, Supplementary Fig. 4B). Therefore, PRAS40 enhances the stemness of CRC-CSCs.

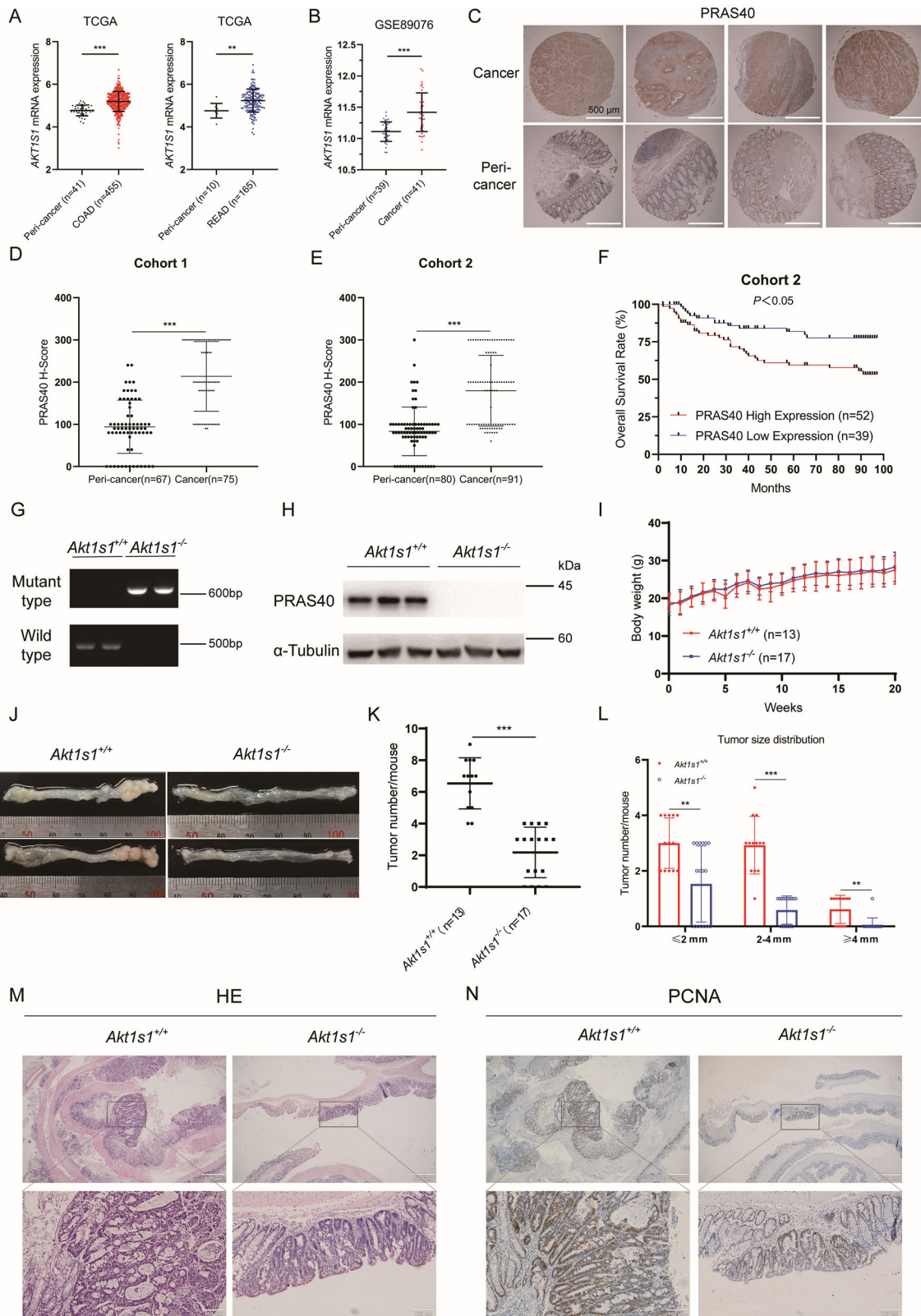
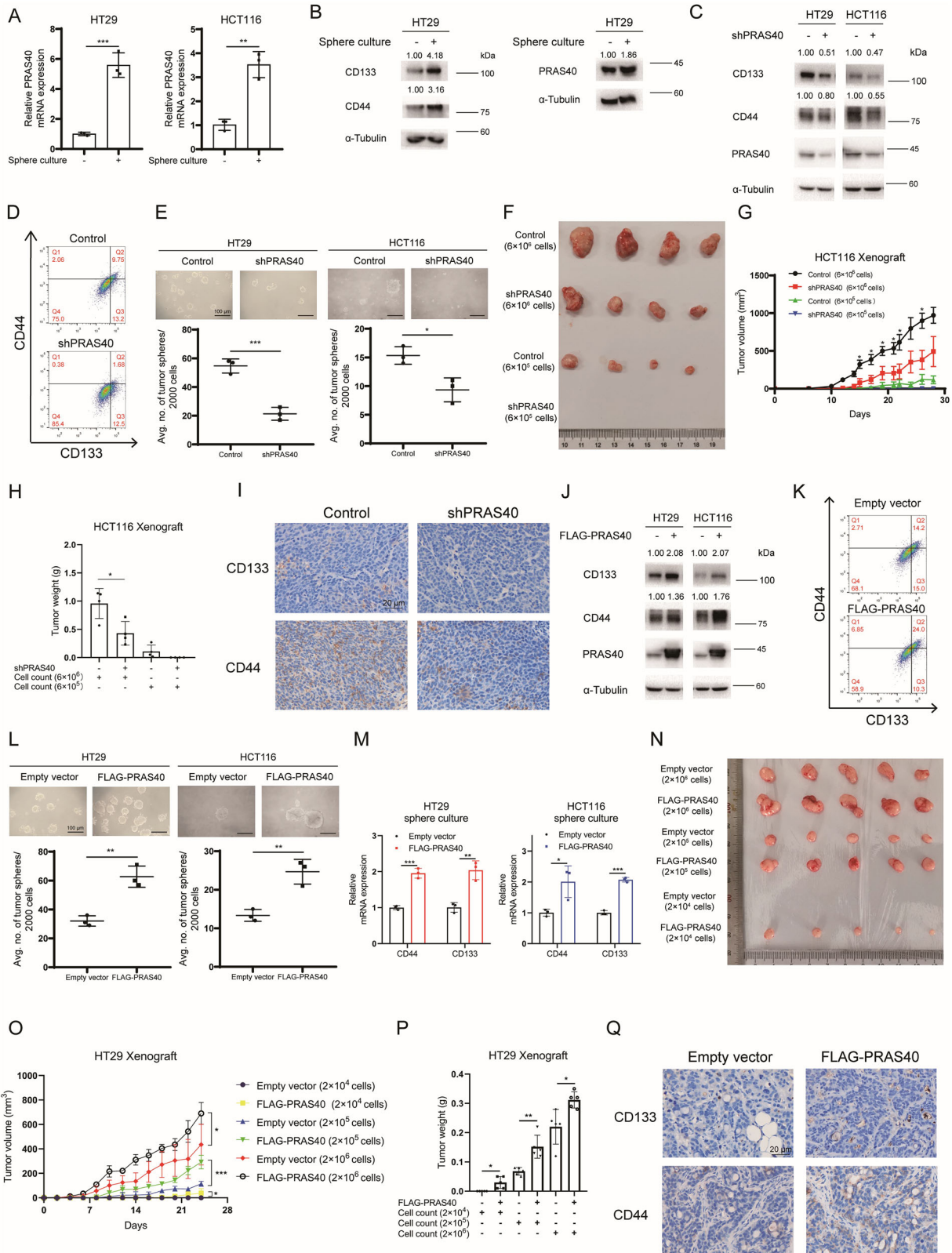


**Fig. 1** Effects of PRAS40 on CRC formation. **A** The expression of *AKT1S1* mRNA in COAD and READ samples from TCGA. **B** The expression of *AKT1S1* mRNA in CRC samples from GSE89076. **C–F** IHC analyses with anti-PRAS40 antibody. Representative images **C**, H-scores **D**, **E**, and overall survival rate of CRC patients **F**. **G–N** colon cancer formation in *Akt1s1*<sup>+/+</sup> and *Akt1s1*<sup>-/-</sup> mice. Genotyping results **G**, western blotting analyses in colon tissues **H**, body weights **I**, representative images **J**, quantitation of tumors **K**, **L**, HE staining **M** and IHC staining with anti-PCNA antibody **N**. Data represent the mean  $\pm$  SD. \*\* $P < 0.01$ ; \*\*\* $P < 0.001$ .



**PRAS40 facilitates the stemness of CRC-CSCs by improving glycolysis**

Given the implication of glycolysis in maintaining CRC stemness [17, 19], and the possible correlation of PRAS40 mRNA expression with the expression of glycolysis-related factors in cCRC [27], we

investigated whether PRAS40 regulates glycolysis in CRC. The results showed that lactate levels were greatly downregulated in the cancer tissues of *Akt1s1*<sup>-/-</sup> mice compared to wild type mice (Fig. 3A). We next altered PRAS40 expression in HT29 and HCT116 cells, and found that glucose consumption and levels of pyruvate

**Fig. 2 Influence of PRAS40 on stemness of CRC cells.** Real time PCR **A** and western blotting analyses **B** in the cells of sphere culture and monolayer culture. **C–I** Cells were introduced with control or PRAS40 shRNA. Western blotting analyses **C**, flow cytometry analyses with anti-CD44 and anti-CD133 antibodies **D**, representative images and quantification of tumor spheres **E**. In vivo tumorigenicity assays were performed. Pictures were taken **F**, tumor volumes were recorded **G**, tumor weights were measured **H**, and CD44 and CD133 were stained **I**. **J–Q** Cells were introduced with empty vector or FLAG-PRAS40 expression vector. Western blotting analyses **J**, flow cytometry analyses with anti-CD44 and anti-CD133 antibodies **K**, representative images and quantification of tumor spheres **L**, real time PCR analyses **M**. In vivo tumorigenicity assays were performed. Pictures were taken **N**, tumor volumes were recorded **O**, tumor weights were measured **P**, and CD44 and CD133 were stained **Q**. Data represent the mean  $\pm$  SD. \* $P < 0.05$ ; \*\* $P < 0.01$ ; \*\*\* $P < 0.001$ . The quantification results of the band density were labeled above the bands.

and lactate were decreased significantly by PRAS40 knockdown, whereas they were increased by PRAS40 overexpression (Fig. 3B–G).

As reported, 2-DG notably inhibited the sphere formation by HT29 cells (Supplementary Fig. 5). Therefore, we used 2-DG to examine whether PRAS40 facilitates the stemness of CRC cells via regulating glycolysis. The sphere formation, the expression of CD133 and CD44, and the proportion of CD133<sup>+</sup>CD44<sup>+</sup> cells facilitated by PRAS40 overexpression were found to be reversed by 2-DG (Fig. 3H–J). However, oxidative phosphorylation inhibitor oligomycin, mitochondrial complex inhibitors rotenone and antimycin A did not eliminate the differences caused by PRAS40 overexpression (Supplementary Fig. 6). Thus, PRAS40 induces glycolysis in CRC cells, which is crucial for the stemness of CRC-CSCs prompted by PRAS40.

#### PRAS40 promotes glycolysis and stemness of CRC-CSCs through activating PGK1

We have previously demonstrated that the glycolytic enzyme PGK1 phosphorylates PRAS40 to inhibit autophagy-mediated cell death in liver cancer cells [25]. PGK1 promotes tumorigenesis by enhancing glycolysis in various cancers, including CRC [28, 30, 32, 34]. However, whether PRAS40 reciprocally regulates glycolysis through modulating PGK1 remains to be elucidated. Results from co-immunoprecipitation (co-IP) assays demonstrated that PGK1 was present in the immunoprecipitates from FLAG-PRAS40-transfected cells but not in those from empty vector-transfected cells (Fig. 4A), indicating that PRAS40 binds PGK1 in HT29 cells. However, PGK1 expression was not affected by either PRAS40 depletion or overexpression (Supplementary Fig. 7). Conversely, we found that the enzymatic activity of PGK1 was significantly decreased upon PRAS40 knockdown but increased upon PRAS40 overexpression (Fig. 4B, C). Additionally, PGK1 knockdown eliminated the increased glucose consumption and lactate production caused by PRAS40 overexpression (Fig. 4D, E). Consistently, the increased proportion of CD133<sup>+</sup>CD44<sup>+</sup> cells and enhanced sphere formation induced by PRAS40 overexpression were also reversed after PGK1 knockdown (Fig. 4F–H). Therefore, PRAS40 increases glycolysis through activating PGK1, ultimately enhancing the stemness of CRC-CSCs.

#### PRAS40 triggers PGK1 acetylation to induce CRC stemness

PGK1 activity is upregulated via acetylation or phosphorylation [29, 31]. To elucidate the mechanism by which PRAS40 promoted PGK1 activity, we investigated whether PRAS40 alters PGK1's acetylation or tyrosine phosphorylation. Immunoprecipitation (IP) results showed that PGK1 acetylation, but not tyrosine phosphorylation, was reduced upon PRAS40 knockdown but increased upon PRAS40 overexpression (Fig. 5A, B).

To further clarify the effects of PRAS40-upregulated PGK1 acetylation on the stemness of CRC-CSCs, we treated CRC cells with the acetylation inhibitors PU139 and anacardic acid. The increased PGK1 activity resulting from PRAS40 overexpression was reversed by both inhibitors (Fig. 5C). Moreover, both inhibitors significantly suppressed the sphere formation, the expression of CD133 and CD44 in both sphere-cultured and monolayer cultured

cells, and the proportion of CD133<sup>+</sup>CD44<sup>+</sup> cells facilitated by PRAS40 overexpression (Fig. 5D–I). These data suggest that PRAS40 facilitates CRC stemness through promoting PGK1 acetylation.

Acetylation of PGK1 can be increased by the acetyltransferase p300/CBP-associated factor (PCAF) and decreased by the deacetylase Sirtuin 7 (SIRT7) [29]. Co-IP results showed that PGK1 binds to PCAF and SIRT7 together with PRAS40 (Fig. 5J). Moreover, the interaction between PGK1 and PCAF was significantly weakened after knocking down PRAS40, while the interaction between PGK1 and SIRT7 was not strengthened (Fig. 5K). In contrast, PRAS40 overexpression improved the interaction of PGK1 with PCAF but did not impair that of PGK1 with SIRT7 (Fig. 5L). Therefore, PRAS40 upregulates PGK1 acetylation via enhancing the interaction between PGK1 and PCAF.

#### Pharmacological inhibition of acetylation impairs CRC stemness and tumorigenesis facilitated by PRAS40 in vivo

Since acetylation inhibitors suppressed PRAS40-induced stemness in CRC cells (Fig. 5), we next explored the possibility of treating CRC in vivo with these inhibitors. HT29 xenografts were established in nude mice using PRAS40-depleted cells reconstituted with FLAG-PRAS40, followed with administration of PU139. Mice receiving PU139 showed no change in body weight (Fig. 6A). PRAS40 reconstitution led to an increase in tumor volumes and weights, which was partially reversed by treatment with 10 mg/kg of PU139 (Fig. 6B–D). Moreover, PGK1 acetylation levels in tumor tissues, elevated by PRAS40 reconstitution, were decreased by PU139 treatment (Fig. 6E). Additionally, lactate levels and the expression of CD133 and CD44, induced by PRAS40 reconstitution, were reduced in the xenograft samples from PU139-treated mice (Fig. 6F, G). Consequently, pharmacological inhibition of acetylation suppresses PRAS40-induced CRC stemness and tumorigenesis in vivo.

#### DISCUSSION

CSCs preferentially utilize glycolysis for energy production, whereas the regulation of glycolysis in these cells remains largely unexplored [11–15]. In this study, we found that PRAS40 promoted CRC carcinogenesis through enhancing the stemness of CRC-CSCs. Mechanistically, PRAS40 facilitated glycolysis by increasing PGK1 activity, which was mediated by the enhancement of PCAF-induced PGK1 acetylation. Acetylation inhibitors suppressed tumor progression driven by PRAS40 overexpression. Therefore, inhibiting PGK1 activity or targeting PRAS40 could represent potential therapeutic strategies for treating PRAS40/PGK1 axis-hyperactivated CRC.

PRAS40 is overexpressed in human HCC and ccRCC, playing crucial roles in tumor initiation and progression [26, 27]. However, the role of PRAS40 in CRC remained to be determined. We found that PRAS40 expression was increased in human CRC, and high expression of PRAS40 positively correlated with poor survival of CRC patients. PRAS40 deletion impaired colorectal carcinogenesis in mice, while PRAS40 knockdown only mildly inhibited the proliferation of monolayer-cultured CRC cells. Although few

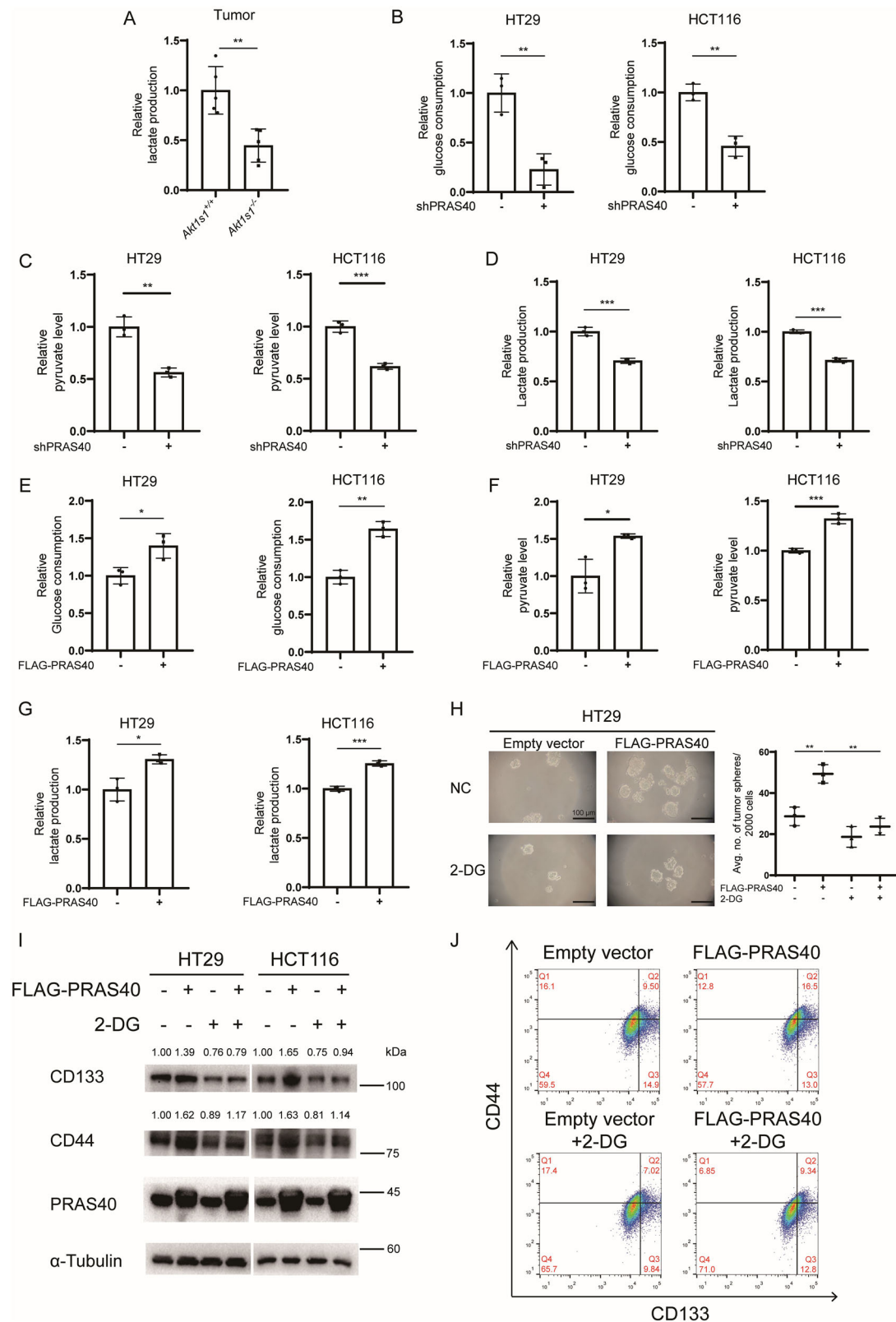


**Fig. 3 Relationship of glycolysis and PRAS40-induced cell stemness.** **A** Lactate levels in tumor tissues of mouse CRC models. **B–D** Cells were introduced with control or PRAS40 shRNA. Analyses of glucose consumption **B**, pyruvate levels **C** and lactate production **D**. **E–G** Cells were introduced with empty vector or FLAG-PRAS40 expression vector. Analyses of glucose consumption **E**, pyruvate levels **F** and lactate production **G**. **H–J** Cells introduced with empty vector or FLAG-PRAS40 expression vector were treated with or without 2-DG (20 mM). Representative images and quantification of tumor spheres were shown **H**. Western blotting analyses **I** and flow cytometry analyses with anti-CD44 and anti-CD133 antibodies **J** were conducted. Data represent the mean  $\pm$  SD. \* $P < 0.05$ ; \*\* $P < 0.01$ ; \*\*\* $P < 0.001$ . The quantification results of the band density were labeled above the bands.

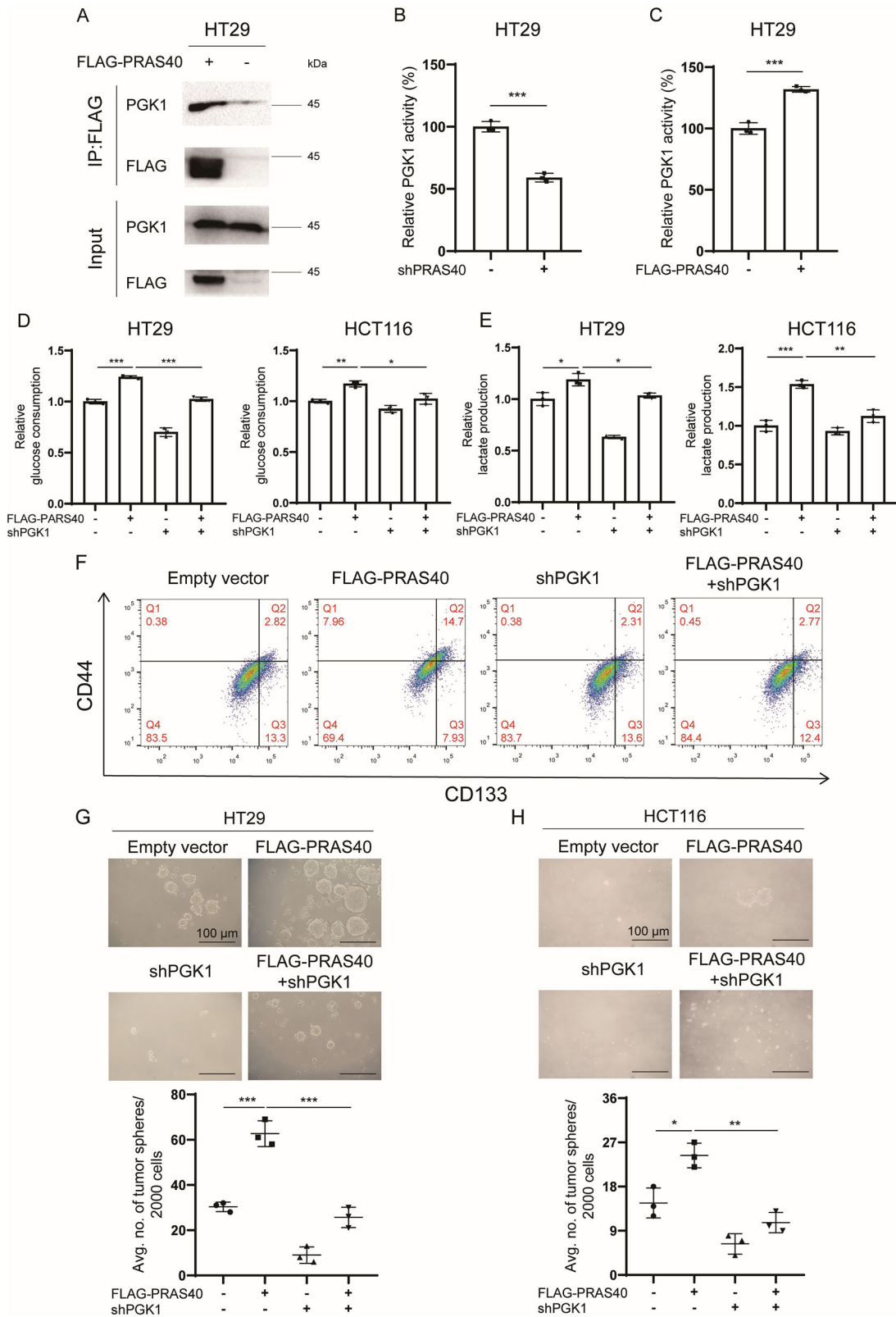


**Fig. 4** Mediation of PRAS40-induced cell stemness by PGK1. **A** Co-IP followed by western blotting analyses in PRAS40-overexpressed HT29 cells. Analyses of PGK1 activity in HT29 cells with PRAS40 knockdown **B** or overexpression **C**. **D–H** HT29 cells were introduced with empty vector or FLAG-PRAS40 expression vector together with control or PGK1 shRNA. Glucose consumption analyses **D**, lactate production analyses **E**, flow cytometry analyses with anti-CD44 and anti-CD133 antibodies **F** were conducted. Representative images and quantification of tumor spheres were shown **G**, **H**. Data represent the mean  $\pm$  SD. \* $P < 0.05$ ; \*\* $P < 0.01$ ; \*\*\* $P < 0.001$ .

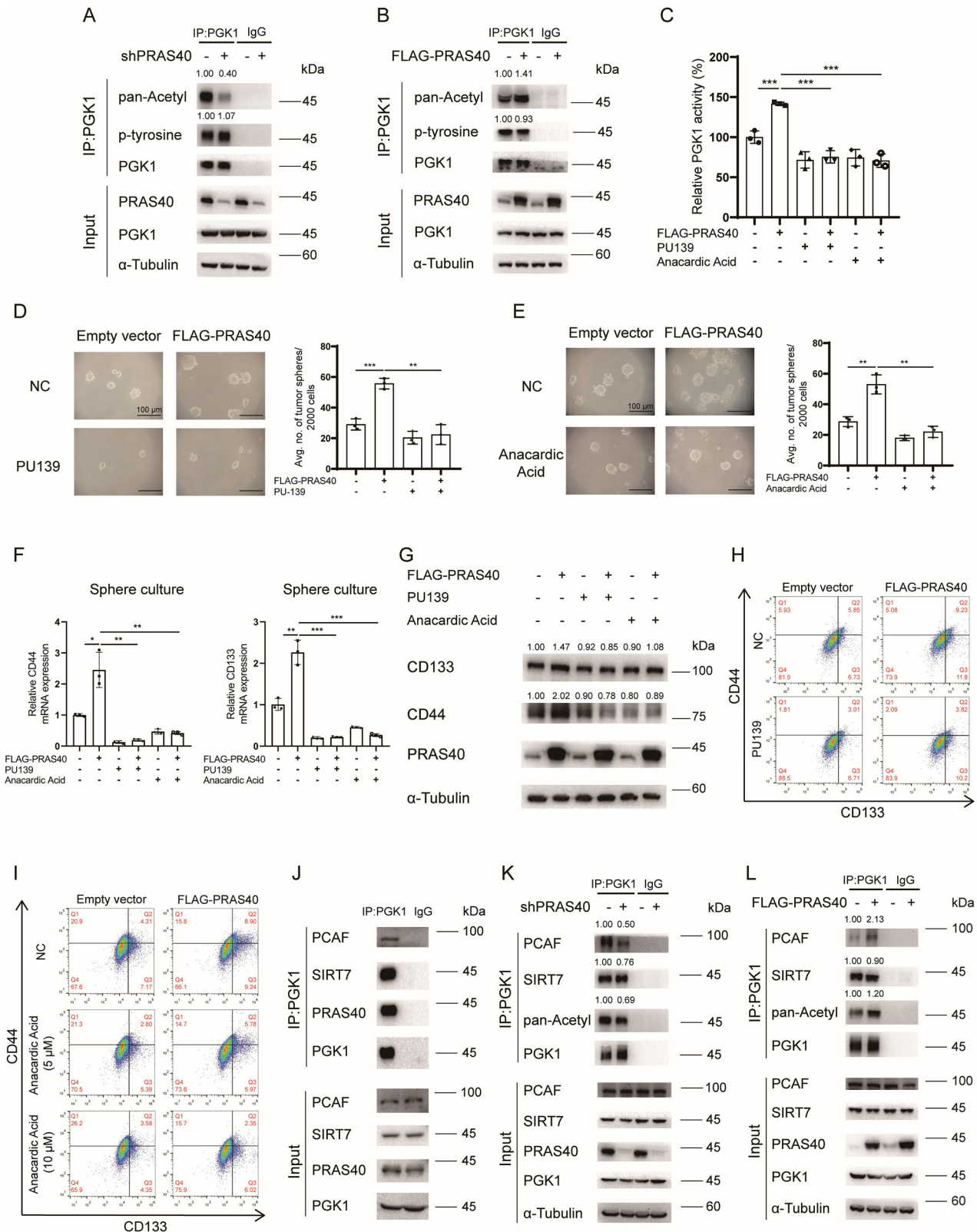


**Fig. 5 Regulation of PGK1 acetylation by PRAS40.** Co-IP followed by western blotting analyses in HT29 cells with PRAS40 knockdown **A** or overexpression **B**. **C–I** HT29 cells were introduced with empty vector or FLAG-PRAS40 expression vector, and treated with or without acetyltransferase inhibitors PU139 (20  $\mu$ M) or Anacardic acid (5 or 10  $\mu$ M). NC, negative control. Analyses of PGK1 activity **C**, representative images and quantification of tumor spheres were shown **D, E**, real time PCR analyses **F**, western blotting analyses **G**, and flow cytometry analyses with anti-CD44 and anti-CD133 antibodies **H, I** were performed. **J** Co-IP followed by western blotting analyses in HT29 cells. Co-IP followed by western blotting analyses in HT29 cells with PRAS40 knockdown **K** or overexpression **L**. Data represent the mean  $\pm$  SD. \*\* $P < 0.01$ ; \*\*\* $P < 0.001$ . The quantification results of the band density were labeled above the bands.

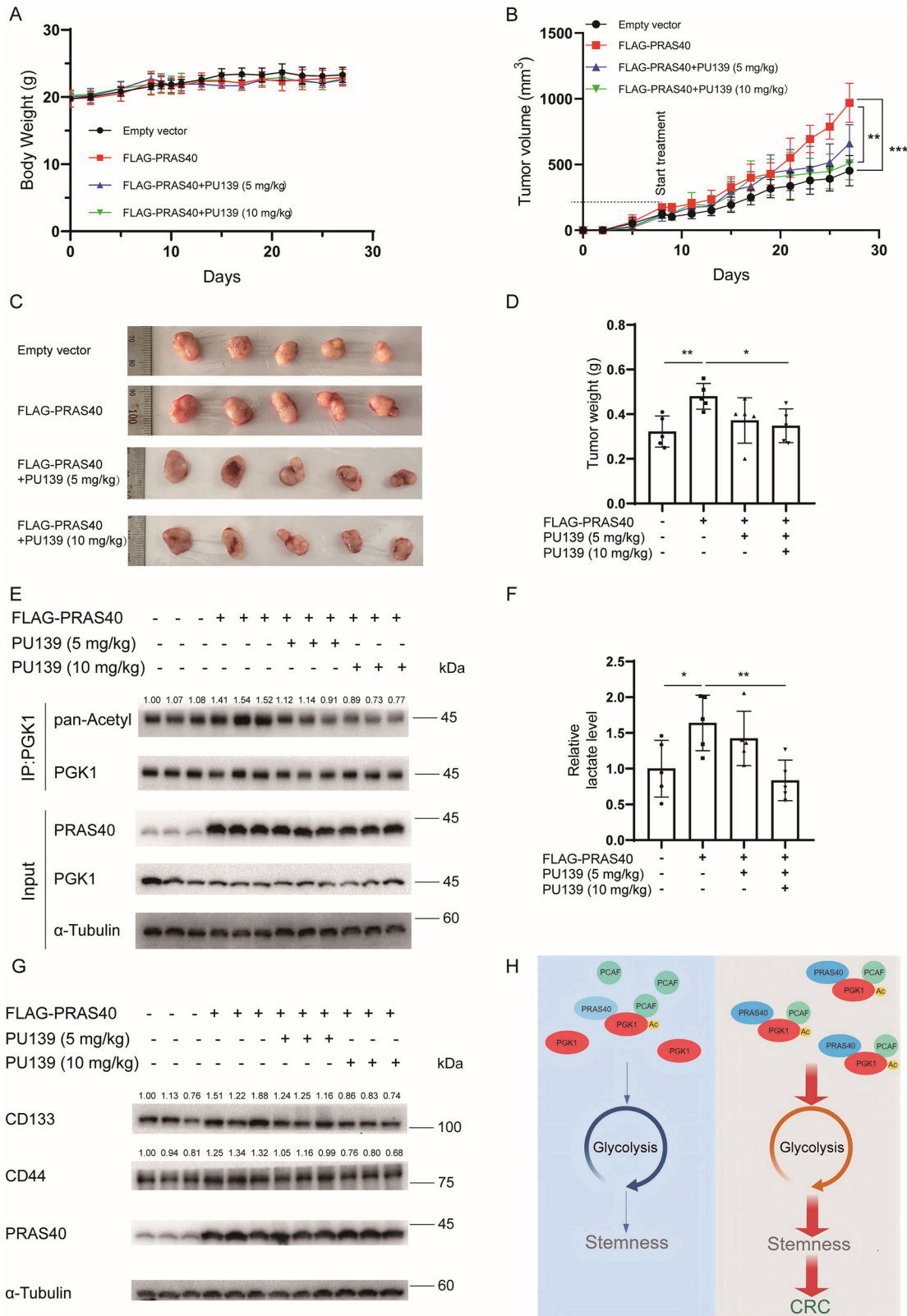


**Fig. 6 Effects of acetylation inhibition on PRAS40-induced cancer cell stemness in vivo.** Xenografts formed in nude mice by PRAS40-depleted HT29 cells reconstituted with empty vector or FLAG-PRAS40 were injected with or without PU139 (5 or 10 mg/kg). **A** Body weights. **B** Tumor volumes. **C** Tumor images. **D** Tumor weights. **E** IP and western blotting analyses of tumors. **F** Lactate levels in tumors. **G** Co-IP and western blotting analyses of tumors. **H** Schematic graphs. The quantification values of the band density were labeled above the bands. Data represent the mean  $\pm$  SD. \* $P < 0.05$ ; \*\* $P < 0.01$ ; \*\*\* $P < 0.001$ .

previous reports demonstrated the relationship between PRAS40 and cancer stemness, the inconsistency between the effects of PRAS40 on CRC initiation in mice and cell growth in monolayer-cultured cell lines prompted us to explore the possible role of PRAS40 in regulating CRC stemness. The enhancement of sphere formation, the increased proportion of CD133<sup>+</sup>CD44<sup>+</sup> cells, and the stimulation of CRC xenograft formation in mice by PRAS40 overexpression clarified the significance of PRAS40 in maintaining CRC stemness. These data suggest the potential of directly targeting PRAS40 for CRC treatment by suppressing cancer stemness.

Glycolysis is well established as a key metabolic pathway in CRC-CSCs [17, 19]. Interestingly, PRAS40 mRNA is overexpressed in ccRCC and positively correlates with the expression of glycolytic hallmarks, though the underlying mechanism remains unknown [27]. In this study, we found that PRAS40 augmented glycolysis as well as CRC stemness. Importantly, glycolysis inhibition attenuated the PRAS40-driven stemness, indicating that PRAS40 promotes stemness in CRC-CSCs through facilitating glycolysis.

We previously reported that the glycolytic enzyme PGK1 phosphorylates PRAS40 in liver cancer cells, whereas the effects of PRAS40 on PGK1 and glycolysis warranted further investigation [25]. In this study, we found that PRAS40 bound to and activated PGK1 in CRC cells, and PGK1 was essential to PRAS40-induced glycolysis and CRC stemness. However, PRAS40 did not alter the expression of PGK1 but upregulated its enzymatic activity, thereby enhancing glycolysis in CRC cells. Various posttranslational modifications of PGK1 augment its activity and consequently facilitate glycolysis. [29, 31, 32, 34]. Regarding the mechanism by which PRAS40 improved PGK1 activity, we found that PRAS40 augmented the acetylation but not tyrosine phosphorylation of PGK1. Furthermore, PRAS40 regulated the interaction between PGK1 and the acetyltransferase PCAF, but not the deacetylase SIRT7. Thus, PRAS40 stimulates PGK1 activity by facilitating PGK1 acetylation through upregulating the interaction between PGK1 and PCAF. The possibility of whether PRAS40 regulates other modifications of PGK1 controlling its activity is still under investigation.

Based on the essential role of PGK1 acetylation in PRAS40-induced PGK1 activity, glycolysis and CRC stemness, we explored the possibility of targeting CRC with acetylation inhibitors. As a result, pharmacological inhibition of acetylation impaired CRC stemness and tumorigenesis *in vivo*. Therefore, the utilization of acetylation inhibitors in PRAS40/PGK1 axis-hyperactivated CRC is anticipated.

In summary, we identified PRAS40 as an oncogenic candidate in CRC and determined that PRAS40 promoted glycolysis and maintained the stemness of CRC cells. PRAS40 binds to PGK1 and induces its catalytic activity by enhancing PCAF-dependent PGK1 acetylation, thereby activating glycolysis to enhance CRC stemness. Targeting this novel PRAS40/PGK1 regulatory axis may provide promising therapeutic approaches for CRC in the future.

## DATA AVAILABILITY

All data generated or analyzed during this study are included in this published article and its supplementary information files. The following publicly available data sets were used: TCGA-COAD, TCGA-READ, and GSE89076.

## REFERENCES

- Siegel RL, Giaquinto AN, Jemal A. Cancer statistics, 2024. *CA Cancer J Clin*. 2024;74:12–49.
- Xia C, Dong X, Li H, Cao M, Sun D, He S, et al. Cancer statistics in China and United States, 2022: profiles, trends, and determinants. *Chin Med J*. 2022;135:584–90.
- Dekker E, Tanis PJ, Vleugels JLA, Kasi PM, Wallace MB. Colorectal cancer. *Lancet*. 2019;394:1467–80.
- Li J, Ma X, Chakravarti D, Shalpour S, DePinho RA. Genetic and biological hallmarks of colorectal cancer. *Genes Dev*. 2021;35:787–820.
- Loh JJ, Ma S. Hallmarks of cancer stemness. *Cell Stem Cell*. 2024;31:617–39.
- Frank MH, Wilson BJ, Gold JS, Frank NY. Clinical Implications of Colorectal Cancer Stem Cells in the Age of Single-Cell Omics and Targeted Therapies. *Gastroenterology*. 2021;160:1947–60.
- Garza Trevino EN, Quiroz Reyes AG, Rojas Murillo JA, de la Garza Kalife DA, Delgado Gonzalez P, Islas JF, et al. Cell Therapy as target therapy against colon cancer stem cells. *Int J Mol Sci*. 2023;24:8163.
- Wang H, Gong P, Chen T, Gao S, Wu Z, Wang X, et al. Colorectal Cancer Stem Cell States Uncovered by Simultaneous Single-Cell Analysis of Transcriptome and Telomeres. *Adv Sci*. 2021;8:2004320.
- Yang L, Shi P, Zhao G, Xu J, Peng W, Zhang J, et al. Targeting cancer stem cell pathways for cancer therapy. *Signal Transd Target Ther*. 2020;5:8.
- Kong W, Gao Y, Zhao S, Yang H. Cancer stem cells: advances in the glucose, lipid and amino acid metabolism. *Mol Cell Biochem*. 2024;479:2545–63.
- Peng F, Wang JH, Fan WJ, Meng YT, Li MM, Li TT, et al. Glycolysis gatekeeper PDK1 reprograms breast cancer stem cells under hypoxia. *Oncogene*. 2018;37:1062–74.
- Zhu T, Zheng J, Zhuo W, Pan P, Li M, Zhang W, et al. ETV4 promotes breast cancer cell stemness by activating glycolysis and CXCR4-mediated sonic Hedgehog signaling. *Cell Death Discov*. 2021;7:126.
- Bi L, Ren Y, Feng M, Meng P, Wang Q, Chen W, et al. HDAC11 Regulates Glycolysis through the LKB1/AMPK Signaling Pathway to Maintain Hepatocellular Carcinoma Stemness. *Cancer Res*. 2021;81:2015–28.
- Wu C, Zheng C, Chen S, He Z, Hua H, Sun C, et al. FOXQ1 promotes pancreatic cancer cell proliferation, tumor stemness, invasion and metastasis through regulation of LDHA-mediated aerobic glycolysis. *Cell Death Dis*. 2023;14:699.
- Chen Z, He Q, Lu T, Wu J, Shi G, He L, et al. mcPGK1-dependent mitochondrial import of PGK1 promotes metabolic reprogramming and self-renewal of liver TICs. *Nat Commun*. 2023;14:1121.
- Li H, Song J, He Y, Liu Y, Liu Z, Sun W, et al. CRISPR/Cas9 Screens Reveal that Hexokinase 2 Enhances Cancer Stemness and Tumorigenicity by Activating the ACSL4-Fatty Acid beta-Oxidation Pathway. *Adv Sci*. 2022;9:e2105126.
- Zhao Y, Chard Dunmall LS, Cheng Z, Wang Y, Si L. Natural products targeting glycolysis in cancer. *Front Pharmacol*. 2022;13:1036502.
- Zhou H, Jiang Y, Huang Y, Zhong M, Qin D, Xie C, et al. Therapeutic inhibition of PPARalpha-HIF1alpha-PGK1 signaling targets leukemia stem and progenitor cells in acute myeloid leukemia. *Cancer Lett*. 2023;554:215997.
- Sedlak JC, Yilmaz OH, Roper J. Metabolism and Colorectal Cancer. *Annu Rev Pathol*. 2023;18:467–92.
- Fonseca BD, Smith EM, Lee VH, MacKintosh C, Proud CG. PRAS40 is a target for mammalian target of rapamycin complex 1 and is required for signaling downstream of this complex. *J Biol Chem*. 2007;282:24514–24.
- Oshiro N, Takahashi R, Yoshino K, Tanimura K, Nakashima A, Eguchi S, et al. The proline-rich Akt substrate of 40 kDa (PRAS40) is a physiological substrate of mammalian target of rapamycin complex 1. *J Biol Chem*. 2007;282:20329–39.
- Wang L, Harris TE, Lawrence JC Jr. Regulation of proline-rich Akt substrate of 40 kDa (PRAS40) function by mammalian target of rapamycin complex 1 (mTORC1)-mediated phosphorylation. *J Biol Chem*. 2008;283:15619–27.
- Sancak Y, Thoreen CC, Peterson TR, Lindquist RA, Kang SA, Spooner E, et al. PRAS40 is an insulin-regulated inhibitor of the mTORC1 protein kinase. *Mol Cell*. 2007;25:903–15.
- Vander Haar E, Lee SI, Bandhakavi S, Griffin TJ, Kim DH. Insulin signalling to mTOR mediated by the Akt/PKB substrate PRAS40. *Nat Cell Biol*. 2007;9:316–23.
- Zhang T, Wang Y, Yu H, Zhang T, Guo L, Xu J, et al. PGK1 represses autophagy-mediated cell death to promote the proliferation of liver cancer cells by phosphorylating PRAS40. *Cell Death Dis*. 2022;13:68.
- Qi Z, Zhang T, Song L, Fu H, Luo H, Wu J, et al. PRAS40 hyperexpression promotes hepatocarcinogenesis. *EBioMedicine*. 2020;51:102604.
- Zhou J, Zhu Y, Liu Y, Niu P, Chen H, Deng J, et al. High PRAS40 mRNA expression and its role in prognosis of clear cell renal cell carcinoma. *Transl Androl Urol*. 2020;9:1650–60.
- Nie H, Ju H, Fan J, Shi X, Cheng Y, Cang X, et al. O-GlcNAcylation of PGK1 coordinates glycolysis and TCA cycle to promote tumor growth. *Nat Commun*. 2020;11:36.
- Hu H, Zhu W, Qin J, Chen M, Gong L, Li L, et al. Acetylation of PGK1 promotes liver cancer cell proliferation and tumorigenesis. *Hepatology*. 2017;65:515–28.
- Liang C, Shi S, Qin Y, Meng Q, Hua J, Hu Q, et al. Localisation of PGK1 determines metabolic phenotype to balance metastasis and proliferation in patients with SMAD4-negative pancreatic cancer. *Gut*. 2020;69:888–900.
- Qian X, Li X, Shi Z, Xia Y, Cai Q, Xu D, et al. PTEN Suppresses glycolysis by dephosphorylating and inhibiting autophosphorylated PGK1. *Mol Cell*. 2019;76:516–27.e7.
- Zhang Y, Yu G, Chu H, Wang X, Xiong L, Cai G, et al. Macrophage-Associated PGK1 Phosphorylation promotes aerobic glycolysis and tumorigenesis. *Mol Cell*. 2018;71:201–15.e7.

33. Li X, Jiang Y, Meisenhelder J, Yang W, Hawke DH, Zheng Y, et al. Mitochondria-Translocated PGK1 Functions as a Protein Kinase to Coordinate Glycolysis and the TCA Cycle in Tumorigenesis. *Mol Cell*. 2016;61:705–19.
34. Liu H, Chen X, Wang P, Chen M, Deng C, Qian X, et al. PRMT1-mediated PGK1 arginine methylation promotes colorectal cancer glycolysis and tumorigenesis. *Cell Death Dis*. 2024;15:170.
35. Xu M, Liu X, Zhou X, Qin Y, Yang L, Wen S, et al. Hypoxia-induced circSTT3A enhances serine synthesis and promotes H3K4me3 modification to facilitate breast cancer stem cell formation. *Pharmacol Res*. 2023;197:106964.
36. Tang W, Wu Y, Qi X, Yu R, Lu Z, Chen A, et al. PGK1-coupled HSP90 stabilizes GSK3beta expression to regulate the stemness of breast cancer stem cells. *Cancer Biol Med*. 2021;19:486–503.
37. Wu D, Lv D, Zhang T, Guo L, Ma F, Zhang C, et al. Antitumor effects of beta-lemene via targeting the phosphorylation of insulin receptor. *Endocr Relat Cancer*. 2019;26:187–99.

## ACKNOWLEDGEMENTS

pLKO.1-shPGK1 was kindly provided by Dr. Daming Gao from Chinese Academy of Sciences. We thank all the Huang laboratory members for the kind support.

## AUTHOR CONTRIBUTIONS

CZ, YB and LH designed research; CZ, YB, TZ, XC, TZ, HT, YW, YL, JS, LW, XW and LH performed the experiments and analyzed the data; CZ and LH wrote the manuscript.

## FUNDING

This work was supported by National Natural Science Foundation of China (81772971) to L Huang and (82203283) to T Zhang, Department of Science and Technology of Liaoning Province (2025JH2/101800250) to L Huang, (2024-BS-187) to T Zhang, and (2025-BSLH-109) to Y Luo, and Department of Education of Liaoning Province (LJ212510161011) to H Teng.

## COMPETING INTERESTS

The authors declare no competing interests.

## ADDITIONAL INFORMATION

**Supplementary information** The online version contains supplementary material available at <https://doi.org/10.1038/s41389-025-00594-x>.

**Correspondence** and requests for materials should be addressed to Lihui Wang, Xiuli Wang or Lin Huang.

**Reprints and permission information** is available at <http://www.nature.com/reprints>

**Publisher's note** Springer Nature remains neutral with regard to jurisdictional claims in published maps and institutional affiliations.



**Open Access** This article is licensed under a Creative Commons

Attribution-NonCommercial-NoDerivatives 4.0 International License, which permits any non-commercial use, sharing, distribution and reproduction in any medium or format, as long as you give appropriate credit to the original author(s) and the source, provide a link to the Creative Commons licence, and indicate if you modified the licensed material. You do not have permission under this licence to share adapted material derived from this article or parts of it. The images or other third party material in this article are included in the article's Creative Commons licence, unless indicated otherwise in a credit line to the material. If material is not included in the article's Creative Commons licence and your intended use is not permitted by statutory regulation or exceeds the permitted use, you will need to obtain permission directly from the copyright holder. To view a copy of this licence, visit <http://creativecommons.org/licenses/by-nc-nd/4.0/>.

© The Author(s) 2025